RSC Advances

ROYAL SOCIETY OF CHEMISTRY

www.rsc.org/advances

Journal Name

RSCPublishing

COMMUNICATION

Nonlinear optical properties of Au/Ag alloyed nanoboxes and their applications in both *in vitro* and *in vivo* bioimaging under long-wavelength femtosecond laser excitation

Cite this: DOI: 10.1039/xoxxoooooox

Received ooth January 2012,
Accepted ooth January 2012

DOI: 10.1039/xoxxoooooox

www.rsc.org/

Kanghui Li, Yalun Wang, Fuhong Cai, Jiaxin Yu, Shaowei Wang, Zhenfeng Zhu, Liliang Chu, Hequn Zhang, Jun Qian*,Sailing He *

We synthesize Au/Ag alloyed nanoboxes (ANBs) with different LSPR (localized surface plasmon resonance) peak wavelengths and observe their various nonlinear optical properties. Both *in vitro* and *in vivo* bioimaging results show that Au/Ag ANBs are very good candidates for high-contrast and deep-tissue nonlinear optical imaging with negligible photothermal toxicity.

Metal nanoparticles (NPs) have received much attention along with the rapid development of nanotechnology and biophotonics in recent years.[1-4] Many kinds of metal nanoparticles such as Au nanospheres,[5,6] Ag nanospheres,[7,8] Au nanorods [9-16] and Au nanocubes[17] have been studied due to their distinctive localized surface plasmon resonance (LSPR) properties, as well as applications in various areas such as bioimaging,[18] biosensing,[19,20] photothermal therapy[21] etc. Despite of their splendid merits, metal NPs still have some limitations. For example, pure Ag nanoparticles are liable to be oxidized. LSPR wavelength of Au nanospheres could only be tuned in a quite narrow region. The synthesis process of Au nanorods usually costs several hours and is very time-consuming. Furthermore, the main LSPR peak of Au nanorods are difficult to tune to shorter than 600nm. Therefore, the appearance of Au/Ag alloyed nanoboxes (ANBs), which belong to "hollow structures" in the "period table" of plasmonic atoms,[29] has attracted a lot of attention due to their amazing properties and fascinating potential application.[22,23] In the present paper, we synthesize Au/Ag alloyed nanoboxes with different LSPR peak wavelengths, and study their nonlinear optical properties and applications in both *in vitro* and *in vivo* bioimaging under long-wavelength femtosecond laser excitation. Here we list some advantages of our approach. Firstly, the whole synthesis process is pretty quick, only costs less than an hour. The synthesis is performed at room temperature by using water as a solvent, and no heating equipment is required. Thus the whole procedure is quite straightforward. Secondly, by controlling the quantity of Ag seeds and the amount ratio of Au to Ag[24], the peak LSPR wavelength of ANBs can be easily tuned in a very wide range [500-1450 nm in our case, from visible to near infrared (NIR)], which is much broader than that of most existing metal NPs. Thirdly, the surface of as-synthesized ANBs is almost "naked", and consequently it is very convenient to graft various functional groups on ANBs, which is very helpful to improving the chemical stability, bio-targeting capability, as well as the biocompatibility of nanoprobes. Fourthly, compared with other imaging agents such as organic fluorophores and quantum dots, our ANBs are not susceptible to photobleaching or blinking. Although Au/Ag ANBs have many special advantages, to the best of our knowledge, their nonlinear optical properties have never been studied. Recently, nonlinear optical properties of metal NPs have become a research focus of many groups.[25,26] Using metal NPs for nonlinear optical bioimaging has many outstanding advantages over the commonly used linear optical bioimaging.[18] Since the nonlinear optical signals are generated only at the focal spot of the excitation laser, photobleaching out of focus can be excluded. The frequency-upconverted nonlinear optical signal is free of auto-fluorescence, and the signal to noise ratio of bioimaging can be improved accordingly. The wavelength of femtosecond (fs) excitation [in the NIR region] for nonlinear optical imaging can be far from the LSPR peak wavelength of the metal NPs, so the photothermal effect can be greatly eliminated. NIR fs excitation can also reduce photodamage towards biosamples, as a longer-wavelength photon has a lower energy. Under long-wavelength (e.g., 1280-1560 nm) fs laser excitation, we observe and study in this paper various nonlinear optical properties from Au/Ag ANBs with different LSPR peak

wavelengths, such as third harmonic generation (THG), second harmonic generation (SHG), multi-photon luminescence (MPL) [including three-photon luminescence (3PL) and two-photon luminescence (2PL)]. According to our analysis of THG/SHG intensities under different fs excitation wavelengths, we conclude that the THG/SHG efficiency of the Au/Ag ANBs is closely related with their LSPR effect. Surface functionalized Au/Ag ANBs were further used for 3PL microscopy as bright contrast agents. We applied Au/Ag ANBs in both in vitro imaging of cancer cells, as well as in vivo imaging of the ears and brains of mice for the first time, with a fs excitation of 1550 nm, which is very near the optical tissue window ranging from 1600nm to 1800nm.[27] Our experiment results have shown that Au/Ag ANBs are very promising in high-contrast and deep-tissue 3PL bioimaging with negligible photothermal toxicity.

ANBs were synthesized according to a seed-mediated method reported by Aherne et al.[22-24] as depicted in scheme 1. Ag seeds were first produced, and then grown to Ag nanoprisms with the guidance of surfactants. Along with addition of $HAuCl_4$ drop by drop, a small amount of Au firstly deposited at the edges of Ag nanoprisms at the beginning of reaction, and then Au/Ag alloy generated in the galvanic replacement reactions and deposited outside the nanoboxes, finally Ag nanoprisms turned into Au/Ag ANBs with a hollow cavity in the interior. [30]The morphology of ANBs was normally of triangle, but when the LSPR wavelength of ANBs was tuned towards a shorter wavelength, they gradually lose their triangular shape. On the contrary, when the LSPR wavelength was tuned towards a longer wavelength, the triangular shape became distinct though the angles were a bit blunt.

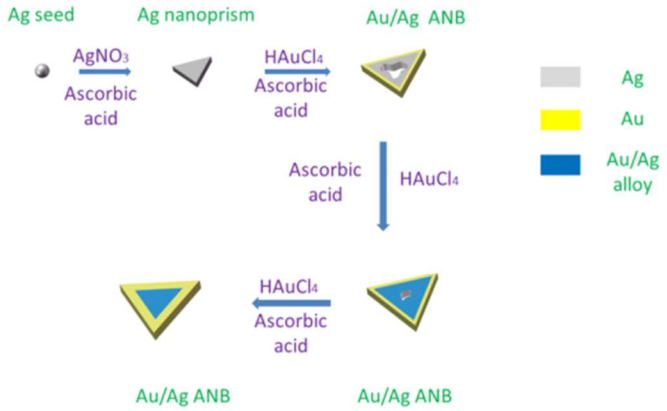

Scheme 1 Growing process of ANB.

Typical structures of ANBs were shown in Figure 1a-d). The ratio of nanoboxes to "solid" alloyed particles is very high and the yield of Au/Ag alloyed nanoboxes is more than 95%.The LSPR peak wavelength is tunable from 500 nm to 1450 nm when the side length of ANBs changes from 15 nm to about 400 nm, which illustrates that a longer side length corresponds to a longer peak LSPR wavelength of ANBs. Figure 1e is the tunable extinction spectra of Au/Ag ANBs, with LSPR peak wavelength ranging from 512-1450 nm. Usually, there are two chemical methods to control the LSPR peak wavelength of Au/Ag ANBs. One is rough tuning by changing the amount of Ag seeds in the mixture. The more Ag seeds we added, the shorter the LSPR peak wavelength was. The other method is fine tuning, which is dependent on the amount of $HAuCl_4$. The more $HAuCl_4$ was added, the shorter the LSPR peak wavelength was. In this way, real-time monitoring of LSPR peak wavelength is possible and its accurate tuning can be easily achieved. During the synthesis of ANBs, the amount ratio of Au to Ag we selected was typically between 3:1 to 4:1. When all the Ag (gray part in the scheme) was converted to Au/Ag alloy (blue part), ANBs grew thicker (yellow part) due to the deposition of increasing amount of Au, which made ANBs much more stable.

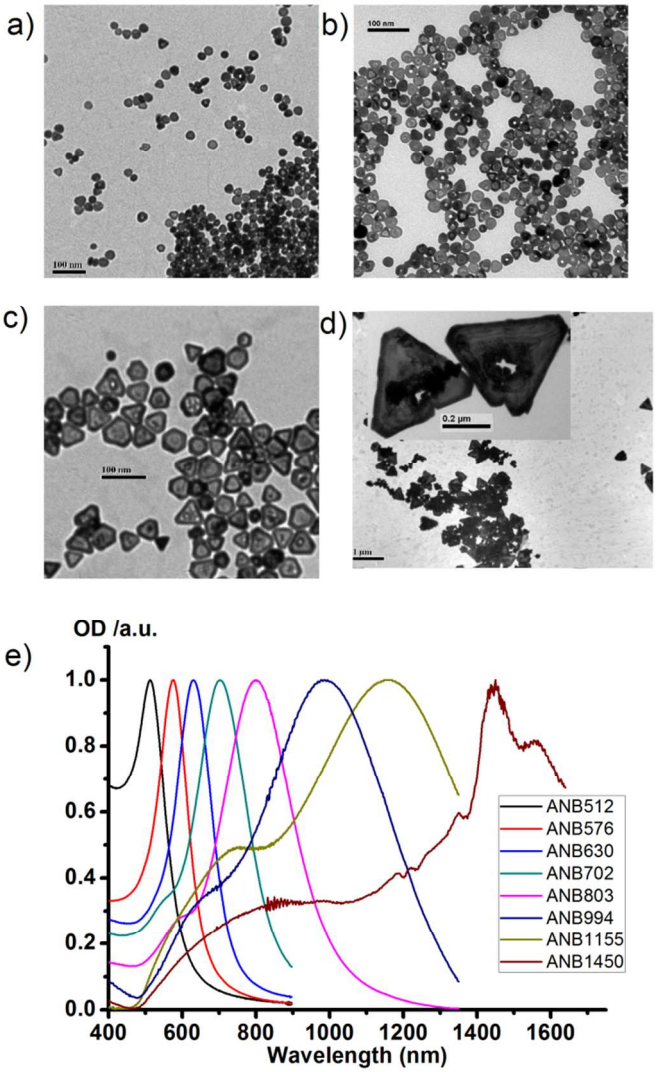

Figure 1 Characterization of Au/Ag ANBs. a-d)TEM images of Au/Ag ANBs with the LSPR peak at 520 nm, 576nm, 702nm, 1450nm respectively, scale bars are 100nm. b) Typical extinction spectra of ANBs, whose LSPR peak wavelengths are indicated by the number in the inset.

To investigate the nonlinear optical properties of Au/Ag ANBs, a home built measurement system was adopted, as depicted in Figure 2a. The fs laser source is the output from an optical parameter oscillator (OPO), which is pumped by a Ti:sapphire fs laser (Mira HP, Coherent, Inc.). Its wavelength can be tuned from 1100 nm to 1580 nm with a repetition rate of 76MHz, and its pulse duration is about 200 fs. To reduce the aggregation-induced LSPR wavelength shift of Au/Ag ANBs, as well as the dipole-dipole interaction among them, Au/Ag ANBs were surface-coated with mPEG-SH (methoxy-poly(ethylene glycol)-thiol) molecules. PEG-coating could keep the dispersibility and stability of ANBs in solution for more than 6months while unmodified ANBs tend to aggregate in less than one week. mPEG-ANBs were then dropped onto a glass slide and dried in a 37 °C oven. The linearly polarized NIR fs laser beam passes through a 1000 nm long-pass filter, and was then converted to a circularly polarized light by a quarter-wave plate (Union Optic, China) to eliminate the background THG from the glass slide or any

other interfaces orthogonal to the optical axis.[26] The laser beam was then directed into a microscope structure and focused onto the sample stage by an aspheric lens. The glass slide was put on the sample stage, and the nonlinear optical signals of ANBs were then excited. The signal was collected along the forward direction through a 40×/0.75 NA object lens (Nikon) and then coupled into a fiber, which was connected to a spectrometer (PG2000, Ideaoptics Instruments, China) for further analysis.

Figure 2b shows the typical emission spectrum of Au/Ag ANBs with an LSPR peak at 520 nm in water (abbreviated as ANB520), which was excited by a 1550 nm-fs laser. As we can see, a strong THG signal (centered at 517 nm) and a relatively weak SHG signal (centered at 775 nm) can be easily discriminated from the spectrum. The apophysis curve between THG and SHG signals is attributed to the 3PL signal from ANBs, while the apophysis longer than 775 nm (the peak wavelength of the SHG signal) is from the 2PL signal of ANBs. Herein, the wavelength of fs excitation we selected is 1550 nm, which is very close to the typical optical tissue window (1600-1800 nm).[27] In this wavelength region, scattering loss of light is very small and the absorption loss of light is not so distinct. Thus, nonlinear optical bioimaging can reach very deep imaging depth, provided that the fs-excitation wavelength is in this optical window. Figure S1 shows the strong nonlinear optical signals from ANBs under the fs excitation of 1650 nm, 1750 nm and 1800 nm, separately, illustrating their promising application prospect in this optical tissue window.

Figure 2c shows the spectra of various THG signals of ANB520 under the fs-excitation ranging from 1360 to 1560 nm. All the THG signals are very distinct, indicating that the THG process of ANBs can respond in a very wide spectral range of excitation. The interaction between light and metal NPs can be dramatically enhanced by the LSPR effect of metal NPs, and it is expected that the THG signal of ANB can also be enhanced by its LSPR effect. To confirm this point, the excitation wavelength of the fs laser was tuned from 1280nm to 1580nm, and the THG intensities of ANB520 were recorded accordingly. Since the intensity of THG is proportional to the cube of the excitation power, we defined a parameter called THG ratio, which is the THG intensity divided by the cube of the excitation power, to describe the THG efficiency at different excitation wavelengths. As shown in Figure 2d, the THG ratio varied at different wavelengths (when tuning the fs-excitation), and the fitting curve of the THG ratio accorded well with the extinction spectrum of ANB520 (in water). Similarly, Figure 2e illustrated various SHG signals of ANB722 under fs excitation, and SHG ratio was defined as the SHG intensity divided by the square of the excitation power, to describe the SHG efficiency at different excitation wavelengths. Figure 2f showed that the fitting curve of the SHG ratio accorded well with the extinction spectrum of ANB722.

These above experimental results illustrated that the existence of the LSPR effect of the ANB did generate the enhancement of its THG/SHG signals, which can be called "LSPR induced THG/SHG enhancement".[7,8] Au/Ag alloyed nanoboxes with LSPR wavelength at the third harmonic/second harmonic of optical excitation could be viewed as nanoscopic optical oscillator of THG/SHG due to LSPR effect, thus their susceptibility $\chi^{(3)}/\chi^{(2)}$ could be dramatically enhanced by the resonance oscillation which lead to enhanced THG/SHG. One thing worth noting is that the strongest THG/SHG appeared when the excitation wavelength was a bit blue-shifted from the triple of 520 nm or the double of 722 nm. It can be explained by the following reason: the peak LSPR wavelength of the ANB sample blue-shifted when their surrounding medium changed from water to air, as they were dried on the glass.

To make full use of ANBs as contrast agents, 3PL (instead of THG and SHG) signals of ANBs were chosen for nonlinear optical bioimaging, for the following two reasons: firstly, 3PL of ANBs is much stronger than their SHG, as depicted in Figure 2b, and thus it could contribute more to the imaging contrast. Secondly, in biological tissue, the attenuation (caused by both absorption and scattering) of light with a wavelength below 600 nm is much larger than that with a wavelength longer than 600 nm. Although the intensity of THG of ANBs is comparable with the intensity of their 3PL, ANB assisted 3PL bioimaging could still achieve deeper-tissue imaging than THG bioimaging. Thirdly, 3PL of Au/Ag alloyed nanoparticles is one order of magnitude stronger than that of pure Au or Ag nanoparticles.[28]

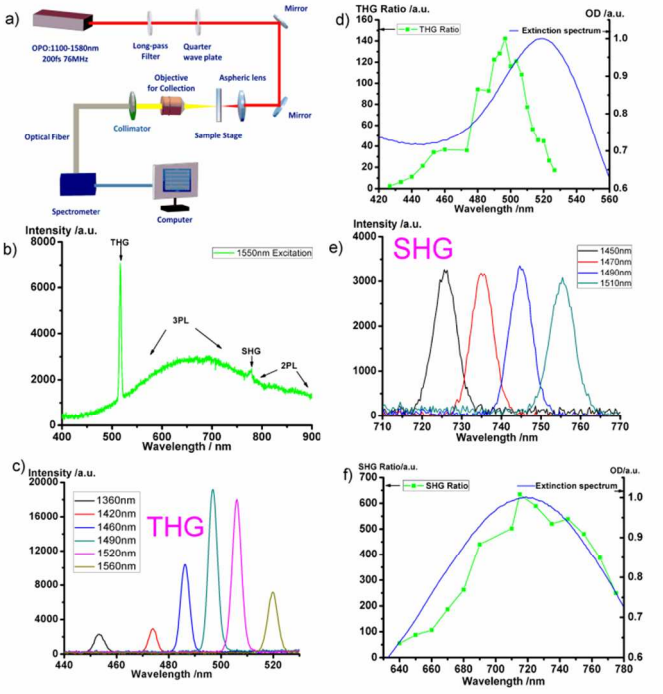

Figure 2 Nonlinear optical properties of Au/Ag ANBs: a) Optical setup for the measurement of the nonlinear optical properties of Au/Ag ANBs. b) A typical emission spectrum of the ANB520 sample when excited by the fs laser at 1550 nm. THG, SHG, 3PL and 2PL signals are all indicated. c) Tunable THG signals of ANB520, when excited by fs laser ranging from 1360 to 1560 nm. d) The curve of THG efficiency is in accordance with the extinction spectrum of ANB520. The green line shows that the THG efficiency varies as the THG wavelength changes (by tuning the fs-excitation wavelength). The blue line shows the extinction spectrum of ANB520. e) Tunable SHG signals of ANB722, when excited by fs laser ranging from 1450 to 1510 nm. f) The curve of SHG efficiency is in accordance with the extinction spectrum of ANB722. The green line shows that the SHG efficiency varies as the SHG wavelength changes .The blue line shows the extinction spectrum of ANB722.

To setup a 3PL scanning microscope, the output of a 1550 nm fs laser source (FLCPA-01C, Calmar Laser, 1 MHz, 400 fs) was

coupled into an upright confocal microscope (Olympus, BX61W1-FV1000), which was equipped with an external photo-multiplier tube (PMT), whose response spectral region was 400 nm~900nm. (See Figure S2 in Supporting Information). To make the ANBs more biocompatible, we made some surface-modification on them (See Scheme S1 in Supporting Information). A549 cells (human lung adenocarcinoma epithelial cell line) were grown on a glass slide. When cells were stained with surface-modified ANB520, the slide was placed upside down on a little well, which was made of PDMS (polydimethylsiloxane) and filled with phosphate buffered saline (PBS, 1X). A 60× oil objective (NA=1.35, OLYMPUS) was adopted to illuminate cells and collect nonlinear optical signals from ANBs. A 590 nm long-pass filter was inserted into the collecting optical path to extract 3PL signals.

Figure 3 illustrated the 3PL images of living A549 cells. According to the 3PL signals from ANBs, we observed that the staining of surface-modified ANB520 on the cells was very uniform and clear. Theoretically speaking, when the wavelength of fs excitation is far away from the LSPR peak wavelength of metal nanoparticles, photothermal effect of metal nanoparticles could be reduced greatly due to the limited light absorption. To study the photothermal effect of ANBs during 3PL imaging process, A549 cells stained with surface-modified ANB520 were continuously scanned by the fs laser and cell images were taken every 5 minutes. It was worth noting that the laser scanning was continuously performed during the whole imaging process, and it did not stop when the cell images were recorded. Figure 3 a-h) illustrated the corresponding experimental results. As we can see, during the first 50 minutes, no obvious transformation of cellular morphologies was observed. The bright spot appeared in Figure 3 g-h) was a gas bubble (outside the cells) caused by photothermal effect. However, the cellular morphologies were still normal even after 70 minutes-scanning, indicating that the photothermal effect of ANB520 had negligible influence on cell health, which was quite important for some bioimaging applications requiring long-term observation. During the whole imaging process, the brightness of 3PL signal from the ANBs did not decrease at all, and this illustrated that the chemical and optical properties of ANBs were very stable under fs excitation with a wavelength of 1550 nm, which was far away from their LSPR peak wavelength.

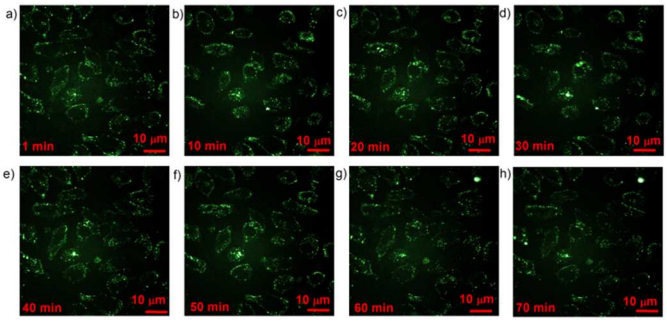

Figure 3 3PL images of A549 cells excited by 1550 nm fs laser. The A549 cells were continuously scanned by 1550 nm fs laser and cell images were recorded every 5 minutes. a-h) were from 1 minute to 70 minute, respectively.

Before in vivo application, we first utilized ANBs for *ex vivo* tissue imaging. PEG-coated ANB520 sample was intravenously injected into a mouse which beared subcutaneous tumor xenografts. 24 hours later, the mouse was sacrificed, and its tumor was taken out. The tumor tissue was fixed, sectioned, and further imaged with the same 3PL scanning microscope (excitation wavelength of fs laser: 1550 nm). Figure 4 shows both transmission and 3PL images of tumor tissue. As can be seen, 3PL signal from ANBs was very strong while the 3PL from tumor tissue was nearly negligible, and the ANBs could be easily discriminated from the background of the tissue, which makes the SNR (signal to noise ratio) of 3PL imaging very high. Furthermore, according to the 3PL images, we know that the accumulation of ANBs in the tumor tissue was quite much, illustrating the potentials of ANBs in tumor targeting, drug delivery, as well as *in vivo* microscopic imaging.

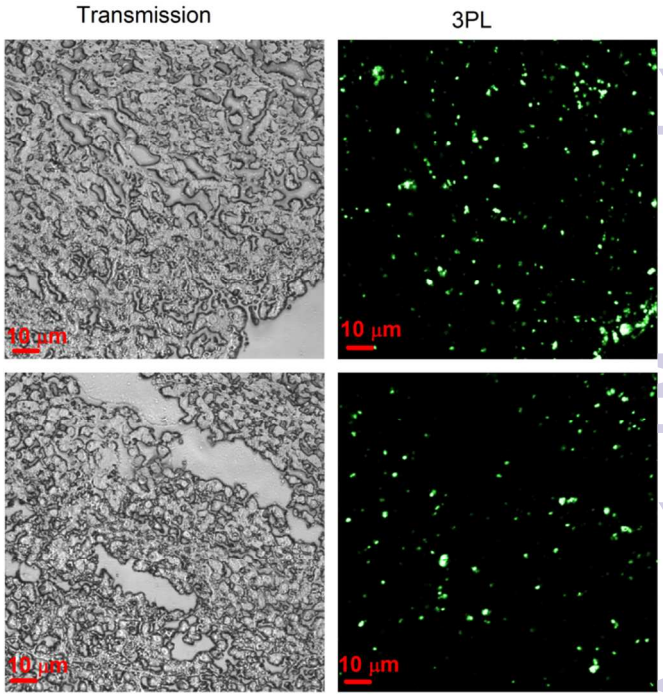

Figure 4 Transmission and 3PL images of tumor tissue targeted with ANB520.

In *in vivo* experiments we adopted the same optical setup as that in *in vitro* and *ex vivo* experiments, and the only difference was that the objective was changed to a 25× water objective (NA=1.05, OLYMPUS), which was specially designed to increase its NIR (e.g. 1550 nm) transmission. Figure 5 a-c) illustrated the 3PL images of ear vasculature of three different mice, which were all intravenously injected with PEG-coated ANB520. As we can see, background noise from ear tissues surrounding blood vessels was negligible, illustrating that ear tissues had very little 3PL. Since the blood vessels were full of intravenously injected ANBs, and the 3PL of ANBs was very strong, the vasculature of ear could be discriminated from surrounding tissues easily under 3PL microscope.

We further utilized PEG-coated ANB520 for 3PL imaging of blood vessels in the brain of a mouse. The mouse was anesthetized, and its skulls were opened up through microsurgery. After intravenously injected with ANBs sample, the mouse brain was imaged with the aforementioned optical setup. Figure 6 shows the 3PL images of brain vasculature at different depth. At superficial tissue, the 3PL signals from blood vessels full of ANBs were very bright, and the SNR of image was very good. When the imaging zone was deeper, the 3PL signals became weaker while the SNR of image got worse, due to the attenuation of the fs excitation in the tissue. However, the brain blood vessles were still distinguishable

from the surrounding tissue even at the depth of 600 μm, indicating the 3PL imaging depth could reach as deep as 600 μm. According to the best of our knowledge, this is the first experiment by using metal nanoparticles for deep 3PL in vivo imaging of a mouse brain. The ANB-based 3PL microscopy will be very helpful in various potential *in vivo* applications (e.g., gene therapy in brain, blood brain barrier penetration, etc.).

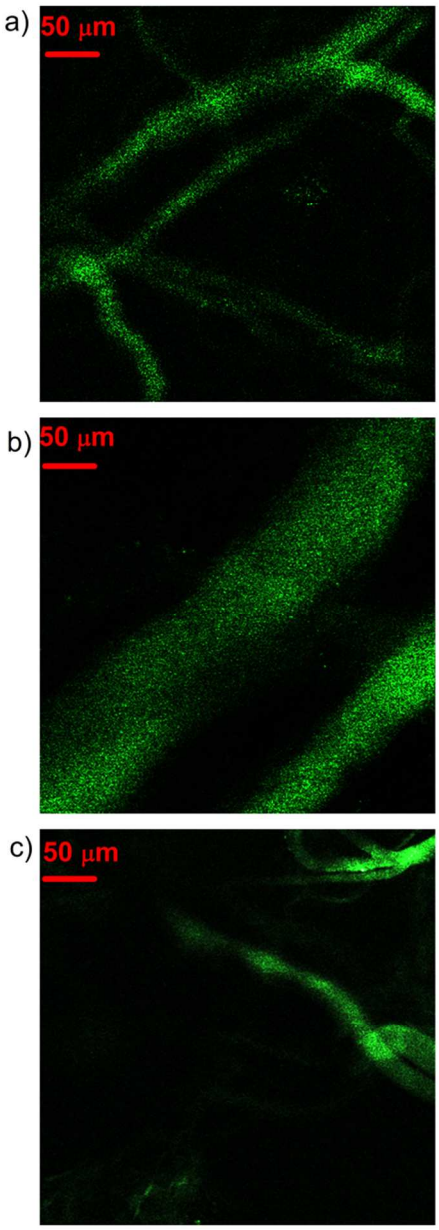

Figure 5 3PL images of the blood vessels of mice. a-c) are from three different mice with ANBs intravenously injected.

Conclusions

In conclusion, we have demonstrated the facile synthesis and characterization of Au/Ag ANBs as novel metal NPs. Under fs laser excitation, Au/Ag ANBs emitted strong and abundant nonlinear optical signals, including THG, SHG, 2PL and 3PL. The variation of THG/SHG intensity of ANBs under fs excitation of different wavelengths showed that the LSPR feature of ANBs could enhance the THG/SHG effect dramatically. With a 1550 nm fs laser based optical scanning microscope, ANBs were further applied in both *in vitro* and *in vivo* 3PL bioimaging. ANBs showed high stability and negligible photothermal effect during 3PL cellular imaging process, which made ANBs very promising in biomedical applications requiring long-term observation. ANBs could also be used as good contrast agents for 3PL in vivo bioimaging, which possesses the advantages of high SNR and deep-tissue imaging capability. ANBs should have great potentials in functional nonlinear optical *in vivo* bioimaging.

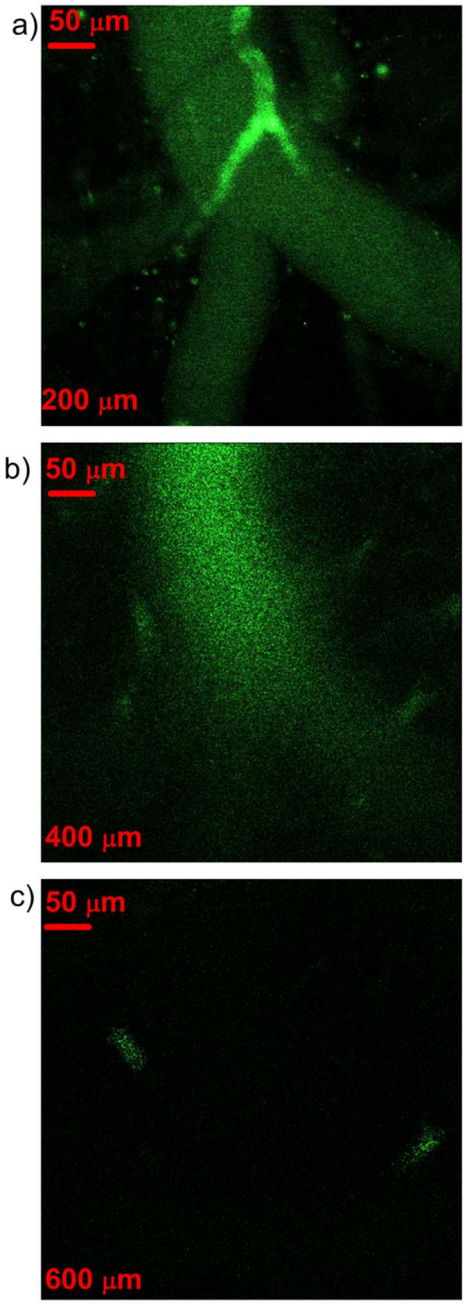

Figure 6. 3PL images of vasculature of a mouse at different depth. a-c) are 200 μm, 400 μm, 600 μm, respectively.

Notes and references

[a] State Key Laboratory of Modern Optical Instrumentation (Zhejiang University), Centre for Optical and Electromagnetic Research, Zhejiang Provincial Key Laboratory for Sensing Technologies, JORCEP (Sino-Swedish Joint Research Center of Photonics), Zhejiang University, Hangzhou, 310058 (China)
E-mail: qianjun@zju.edu.cn; sailing@kth.se.

† Electronic Supplementary Information (ESI) available: [Experimental and additional figures]. See DOI: 10.1039/c000000x/

‡ This work was partially supported by the National Basic Research Program (973) of China (973 Program; 2013CB834704 and 2011CB503700), the National Natural Science Foundation of China (61275190 and 91233208), the Science and Technology Department of Zhejiang Province, and the Fundamental Research Funds for the Central Universities. We want to express our deepest gratitude toward Thorlabs Inc. for their help in terms of scanning microscope. We are also grateful to Prof. M. Hu's group of Tianjin Univ. for help in femtosecond laser.

[1] E. M. Goldys and M. A. Sobhan, *Adv. Funct. Mater.* 2012, **22**, 1906.
[2] P.Zijlstra, James W. M. Chon and M. Gu, *Nature,* 2009,**459**, 410.
[3]Q. Q. Zhan, J. Qian, H. J. Liang,G. Somesfalean, D. Wang, S. L. He, Z. G. Zhang and S. Andersson-Engels, *ACS Nano,* 2011,**5**,3744.
[4]X. Li, L. Jiang, Q. Q. Zhan, J. Qian and S. L. He, *Colloids Surf. A,* 2009, **332**, 172.
[5] H.T. Sun, X. Sun, M. P. Yu, A. K. Mishra, L. P. Huang and J.Lian, *Adv. Funct. Mater.* 2014,**24**,2389.
[6] Z. P. Guan, N. Y. Gao, X. F. Jiang, P. Y. Yuan, F. Han and Q. H. Xu, *J. Am. Chem. Soc.* 2013**, 135**, 7272.
[7]T. M. Liu, S. P. Tai, C. H. Yu, Y. C. Wen, S. W. Chu, L. J. Chen, M. R. Prasad, K. J. Lin and C. K. Sun, *Appl. Phys. Lett.* 2006, **89**, 043122.
[8] S. P. Tai, Y. Wu, D. B. Shieh, L. J. Chen, K. J. Lin, C. H. Yu, S. W. Chu, C. H. Chang, X. Y. Shi, Y. C. Wen, K. H. Lin, T. M. Liu and C. K. Sun, *Adv. Mater.* 2007, **19**, 4520.
[9] C. Kuemin, L. Nowack, L. Bozano, N. D. Spencer and H. Wolf, *Adv. Funct. Mater.* 2012, **22**, 702.
[10] H. F. Wang, T. B. Huff, D. A. Zweifel, W. He, P. S. Low, A. Wei and J. X. Cheng, *Proc.Natl.Acad.Sci.*2005,**102**, 15752.
[11] C. Hubert, L. Billot, P.-M. Adam, R. Bachelot, P. Royer, J. Grand, D. Gindre, K. D. Dorkenoo and A. Fort, *Appl. Phys.Lett.* 2007**, 90**, 181105.
[12] Y. Y. Jung, H.T. Chen, L. Tong and J. X. Cheng, *J. Phys. Chem. C,* 2009,**113**, 2657.
[13] T. Y. Wang, D. Halaney, D. Ho, M. D. Feldman and T. E. Milner, *Biomed. Opt. Express,* 2013, **4**, 584.
[14] H. F. Yuan, S. Khatua, P. Zijlstra, M. Yorulmaz and M. Orrit, *Angew. Chem. Int. Ed.* 2013, **52**, 1217.
[15] N. J. Durr, T. Larson, D. K. Smith, B. A. Korgel and K. Sokolov, A. B. Yakar, *Nano Lett.* 2007, **7**, 941.
[16] Y. Zhang, J. Qian, D. Wang, Y. Wang and S. L. He, *Angew.Chem. Int. Ed.* 2013, **52**, 1148.
[17] H. J. Chen, Z. H. Sun, W. H. Ni, K. C. Woo, H. Q. Lin, L. Q. Sun, C. H. Yan and J. F. Wang, *Small,* 2009, **5**, 2111..
[18] L. Tong and J. X. Cheng, *Mater. Today,* 2011, **14**, 264.
[19] Y. C. Cao, R. C. Jin and C. A. Mirkin, *Science,* 2002, **297**, 1536.
[20] S. Nie and S. R. Emory, *Science,* 1997, **275**, 1102.
[21] L. Gao, J. B. Fei, J. Zhao, H. Li, Y. Cui and J. B. Li, *ACS Nano*, 2012, **6**, 8030.
[22] D. Aherne, M. Gara, J. M. Kelly and Y. K. Gun'ko. *Adv. Funct. Mater.* 2010, **20**, 1329.
[23] D. Aherne, D. M. Ledwith, M. Gara and J. M. Kelly. *Adv. Funct. Mater.* 2008, **18**, 2005.
[24] X. W. Liu, J. Lin, T. F. Jiang, Z. F. Zhu, Q. Q. Zhan, J. Qian and S. He, *Prog. Electromagn. Res.* 2012, **128**, 35.
[25] J. Butet, J. Duboisset, G. Bachelier, I.R. Antoine, E. Benichou, C. Jonin and P. F. Brevet, *Nano Lett.* 2010, **10**, 1717.
[26] O. Schwartz and D. Oron, *Nano Lett.*2009, **9**, 4093.
[27] N. G. Horton, K. Wang, D. Kobat, C. G. Clark, F. W. Wise, C. B. Schaffer and C. Xu, *Nat. Photonics* 2013, **7**, 205.
[28] L. Tong, C. M. Cobley, J.Y. Chen, Y. N. Xia and J. X. Cheng, *Angew. Chem. Int. Ed.* 2010, **49**, 3485
[29]S. J. Tan, M. J. Campolongo, D. Luo and W. L. Cheng, *Nat. nanotech.* 2011, **6**, 268.
[30] W. Xiong, D. Sikdar, M. Walsh, K. J. Si, Y. Tang, Y. Chen, R. Mazid, M. Weyland, I. D. Rukhlenko, J. Etheridge, M. Premaratne, X. Y. Li, and W. L. Cheng. *Chem. Commun.* 2013, **49**, 9630.

